



Analysis of material property models on WAAM distortion using nonlinear numerical computation and experimental verification with P-GMAW

Yupiter H. P. Manurung¹ · Keval P. Prajadhiana¹ · Mohd Shahrman Adenan¹ · Birgit Awiszus² · Marcel Graf³ · Andre Haelsig⁴

Received: 27 June 2020 / Revised: 19 January 2021 / Accepted: 1 February 2021 / Published online: 16 February 2021
© Wrocław University of Science and Technology 2021

Abstract

This fundamental research deals with the investigation of material property model influences on distortion induced by multi-layered Wire Arc Additive Manufacturing (WAAM) with synergic-pulsed gas metal arc welding (P-GMAW) process which was modelled and simulated by means of non-linear numerical computation. The material property models of stainless steel SS316L component to be compared stem from three different sources namely existing database, initial wire and evolved component. The new property models were generated with advanced material modelling software JMATPRO based on chemical compositions analysed at initial wire and component using SEM–EDX. The flow curve for each material model was taken with the strain rates ranging from 0.001 to 1.0 s⁻¹. In the numerical simulation, a coupled thermomechanical solution was adopted including phase-change phenomena defined in latent heat. Goldak’s double ellipsoid was applied as heat source model and simplified rectangular bead with hexagonal element type and meshing was developed to avoid extensive pre-processing effort and to reduce the computational time at post-processing level. Temperature behaviour due to the successive layer deposition was simulated considering heat transfer effect coupled to mechanical analysis. The adjustment of simulative transient to experimental thermal distribution lead to new fitted heat transfer coefficient. Prior to execution of numerical simulation, a sensitivity analysis was conducted to find the optimal number of elements or mesh size towards maximum reached temperature. It can be concluded based on the adjusted model, selected mesh size and experimental validation that numerical computation of substrate distortion with evolved material property of component and initial wire of SS316L yield closer average result within the relative error ranging between 11 and 16% compared to database material giving more than 22%.

Keywords WAAM · Numerical computation · Material property model · Distortion · FEM

1 Introduction

The extensive combination of mathematical modelling as well as advanced numerical techniques by means of computer-aided tool makes a significant impact on optimizing the fundamental of the real process executed within engineering environment. In recent years, engineering research revolving around the usage of numerical computational method had been performed to investigate deformation, microstructures as well as the strength within additively manufactured component [1–3].

The term of Additive Manufacturing (AM) had been in researcher’s radar for the last decade. The concept of AM is to build component by constructing it in a layer to layer manner in contrast to subtractive manufacturing which has

✉ Yupiter H. P. Manurung
yupiter.manurung@uitm.edu.my

¹ Smart Manufacturing Research Institute (SMRI) & Faculty of Mechanical Engineering, Universiti Teknologi MARA (UiTM), Shah Alam, Malaysia

² Professorship of Virtual Production Engineering, Chemnitz University of Technology, Chemnitz, Germany

³ Chair of Materials and Surface Engineering, Chemnitz University of Technology, Chemnitz, Germany

⁴ Chair of Welding Engineering, Chemnitz University of Technology, Chemnitz, Germany

already been executed for many decades. Among the different additive manufacturing techniques, wire and arc additive manufacturing (WAAM) is implemented to produce large metallic part owing to the high deposition rates achieved using an electric arc as the heat source and a solid wire as the feedstock material. This technology can produce large-scale metal components relatively economically. WAAM is a direct feeding process that involves the combination of electric sources, a motion system, and wire based feedstock [4, 5].

For the last several years, the usage of numerical computation using FEM on investigating the behaviour of WAAM process had been executed by numerous researchers in engineering field. An engineering research was performed to show the overall design study for WAAM process modelled within FEM computational model and the main focus was to explore the process capabilities on manufacturing complex product concerning the effect of inter-pass temperature within component [6]. Meanwhile, a research had been performed to optimize the overall computational time of for WAAM model and it also showed the importance of FE analysis usage on modelling the WAAM process in term of overall time consumed [7].

The high deposition rate of WAAM process allows the creation of complex metal component in a flexible manner with high velocity. However, at some cases such flexibility results in large thermal gradients in workpiece causing the emergence of distortion. The involvement of FEM is becoming an essential tool for prediction the level of distortion and residual stress within the WAAM component, which allows the optimization of planning prior to the actual WAAM process which, if executed in correct term, should avoid costly trials [8]. An advanced usage of numerical computation using FEM software has been executed to investigate the distortion [9] and the effects of cooling time applied in the deposition of layers induced during WAAM process [10]. The distortion prediction of WAAM process which utilizes the numerical computational model was conducted [11]. A thermo-mechanical modelling for WAAM process by utilizing commercial-based software for semi-finished product which investigates the influence of wire feed speed and the temperature distribution was performed and the results showed that the orientation position of bead deposition had critical influence on temperature distribution as well as the component geometry [12].

Several researchers conducted investigations to find methods to improve the results and to mitigate the distortion [13, 14]. An investigation was also carried out on the determination of mesh size which can be sensitive to the result [15]. Material properties played a significant role in the numerical simulation to obtain better final distortion magnitude [16]. Studies focusing on material modelling showed the importance of material data as one of crucial factors to

improve simulation results [17]. A similar research was also performed concerning about how the improved material modelling in welding process study could lead into a better result when compared to real engineering application [18]. Other research also concerned the property evolutions within material modelling on designing the numerical simulation model [19]. Optimized process control had been performed to study deformation behaviour on WAAM components which changed the final geometrical shape of the desired products [20, 21].

To improve metallurgical and mechanical properties at welded joint, some researcher investigated the major parameters using pulsed-current welding process. It is found that grain size can be controlled using this welding method due to adjustment of cooling rate [22]. The proper selection of pulse parameters will give outstanding bead geometry, melting rate and arc stability. It is also shown that the electrode melting rate in pulsed current welding is higher than continuous one under similarly equivalent current. This may lead to less time in weld joint preparation [23].

Reviewing previous researches which revolved around WAAM, it is found out, that there were less attempts executed on investigating the effect of material property model towards the deformation of WAAM component using P-GMAW process. This research focuses on developing a hollow rectangular shape with twenty-five layers, in which the effect of the difference in material modelling based on three conditions, namely existing material database, initial and deposited wire was investigated with regard to their influence on the deformation occurred on the substrate. Apart from point-by-point, the total deformation of substrate material SS304 was analysed between simulation and experiment.

2 Experimental set-up and procedures

The rectangular WAAM shape was built using a series of experiments using robotic welding system with pulsed power source (GMAW) and filler wire of stainless steel SS316L ($\varnothing 1.2$ mm). As the substrate, a plate of commercially available stainless-steel plate SS304 with dimension of 140 mm (l) \times 60 mm (w) \times 4 mm (t) was to be analysed. The deposition consisted of 25 layers of beads forming a hollow rectangular shape on the substrate. This experimental study utilized robotic welding equipment ABB IRB 2400/16 along with its power source KEMMPI Pro Evolution ProMIG 540MXE embedded to the robotic welding components.

In improving weld characteristic and material property, the advantages of P-GMAW over GMAW are due to the capability of precisely regulating thermal and transfer behaviour of metal deposition which depends upon the proper control of pulse welding parameters. The synergic power



Fig. 1 ABB IRB 2400/16 Robotic welding Machine (left) and KEMMPI ProMig 540 MXE (right)

Table 1 Experimental P-GMAW Parameters for twenty-five layers hollow WAAM

Experimental parameters	Value
Current (A)	85–91
Background/peak current (A)	35/210
Voltage (v)	14–26
Welding speed (mm/s)	7
Wire feed rate (m/min)	3
Wire type and dimension	SS316L ($\varnothing d = 1.2$ mm)
Shielding gas composition	100% Argon
Number of layers (-)	25
Avg. height/width/thickness of component (mm)	37.5/25 /3.75
Measurement uncertainty	± 0.1

source system was equipped with built-in program for selecting parameters which was generally based on diameter and material of filler wire. In this experiment, P-GMAW was used for the 25-layers of hollow WAAM processes with the assigned parameters such as voltage (V), arc current (I),

travel speed and wire feed speed. The current here were set based on the principal of synergic-pulsed GMAW process which constantly switches between low (background) to high (peak) amperage set within power source. The duty cycle of the pulse was approximately 30%. The robotic welding system is shown in Fig. 1 below.

Table 1 below lists the parameters for the experimental WAAM process.

The calibration method for this study was executed by means of thermal calibration process using the comparison of temperature distribution. The data logger ALMEMO 2890–9 recorded the temperature distribution over the course of twenty-five-layer depositions which were to be compared with the temperature distribution of WAAM simulation process. Figure 2 shows the Thermocouples type K within the WAAM experiment and the result of the temperature–time behaviour at a particular location.

Distortion measurement using Coordinate Measuring Machine (CMM) Mitutoyo beyond 707 with accuracy of one micron was chosen which was executed twice on several exactly similar locations of each specimens prior to and after experiment. The difference of measurement value gave the distortion occurred on the measurement points. The experimental WAAM was further analysed using SEM–EDX microscope to extract the chemical composition for material modelling feature implemented in numerical computation analysis. The SEM–EDX Hi-Tech Instrument SU3500 was used to investigate the material composition of initial wire or component (Oerlikon Inertfil 316LSi) and component. Figure 3 shows the specimen sample and results using SEM/EDX.

The noticeable difference in chemical composition can be spotted in three different material models on chemical composition shown in Table 2. It can be observed that there are slight differences before and after WAAM process. Some loses of Ni, Si and Ti could happen during the process. These elements could be formed in the fume emissions and parts of slag on the component surface.

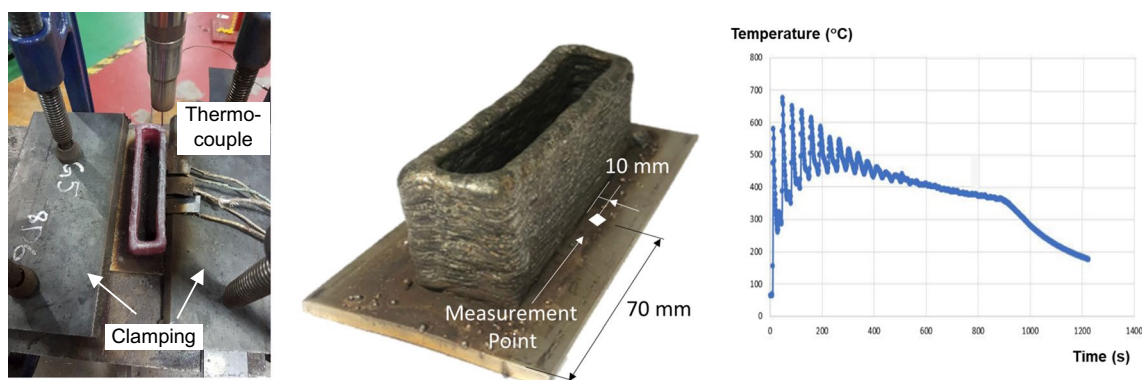


Fig. 2 Temperature measurement and result using Thermocouple type K placed in the 10th layer

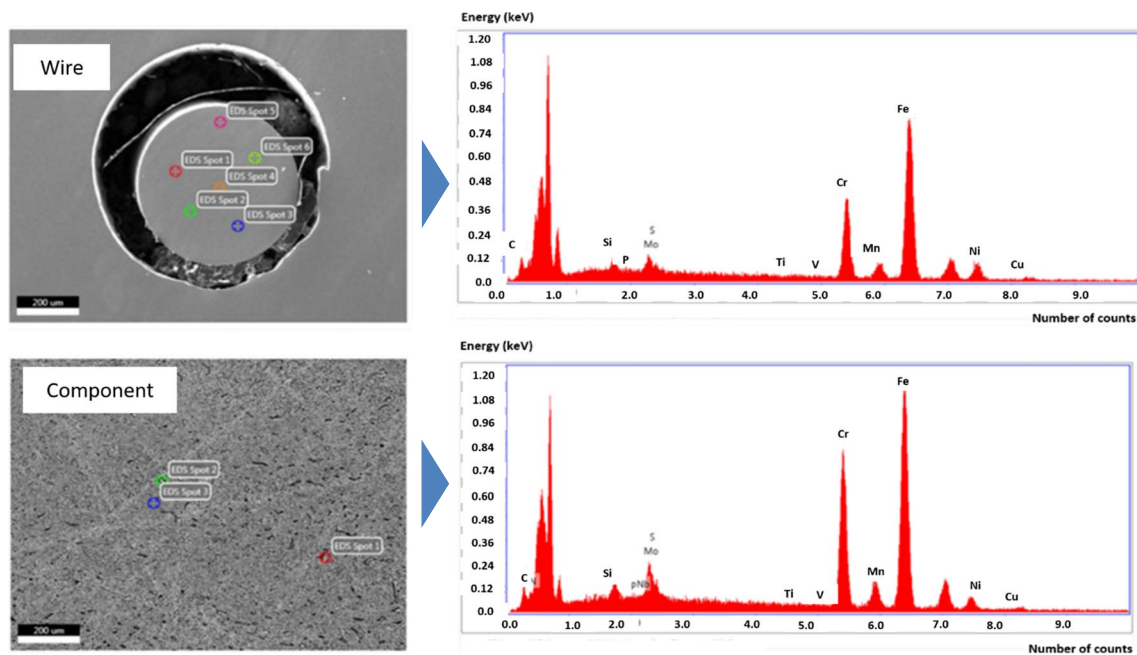


Fig. 3 Spots and Results of chemical composition using SEM–EDX on wire and component

Table 2 Average chemical compositions of SS316L

Material	C	Cu	Cr	Mn	Mo	N	Ni	S	Si	Ti	V	P
Wire	0.01	0.9	17.26	2.46	1.66	0.05	11.36	–	0.76	0.34	0.38	0.02
Component	0.03	0.76	17.83	2.43	1.63	–	10.57	–	0.63	0.267	0.3	–
Database	0.018	–	16.63	2.05	1.57	0.0153	11.18	0.002	0.48	–	–	0.04

3 Computational modelling and simulation of WAAM process

Modelling and simulation of hollow-shaped WAAM process was based on sequentially coupled transient thermo-mechanical FEM using MSC Marc/Mentat in which the temperature distribution was calculated first and then the results are applied to the mechanical analysis. The filler material was modelled with different material models and simulated by means of inactive element method. Commonly used heat source model for GMAW process was used to apply the heat to the additively manufactured deposits which also considered the heat loss through convection to solid elements and to surrounding as well as radiation from free surfaces. The clamping was also modelled following actual location in experiment.

3.1 Geometrical and material modelling

The geometrical model for this WAAM component was a thin-wall component with hollow rectangular shape with

dimension of 105 (l) × 25 (w) × 37.5 (h) mm and thickness of 3.75 mm fabricated on a thin plate as substrate with dimension of 140 (l) × 60 (w) × 4 (t) mm made of stainless-steel material SS304 similar to experiment. The component consisted of twenty-five deposited layers. Component, substrate and table were discretized with hexagonal element. The selection of simplified rectangular instead of arc mesh element form for component was purposely aimed to reduce pre and post processing time. The clamping model is located on both edges of substrate. Figure 4 shows the FE model with 25 deposited layers.

In many manufacturing simulation areas, the method of extracting the material data from EDX to be implemented within numerical computation had been performed in number of investigations [24, 25]. This simulation assigned austenitic stainless-steel material for filler (SS316L) and substrate (SS304). The material modelling for filler material SS316L method is based on the chemical composition shown in Table 2 and generated using material software JMATPRO, while for substrate from material database of software. Figure 5 displays the temperature-dependant properties of SS316L which are thermal expansion coefficient, thermal conductivity, Young's modulus and specific heat

Fig. 4 Actual Specimen and FE model of 25 layers WAAM

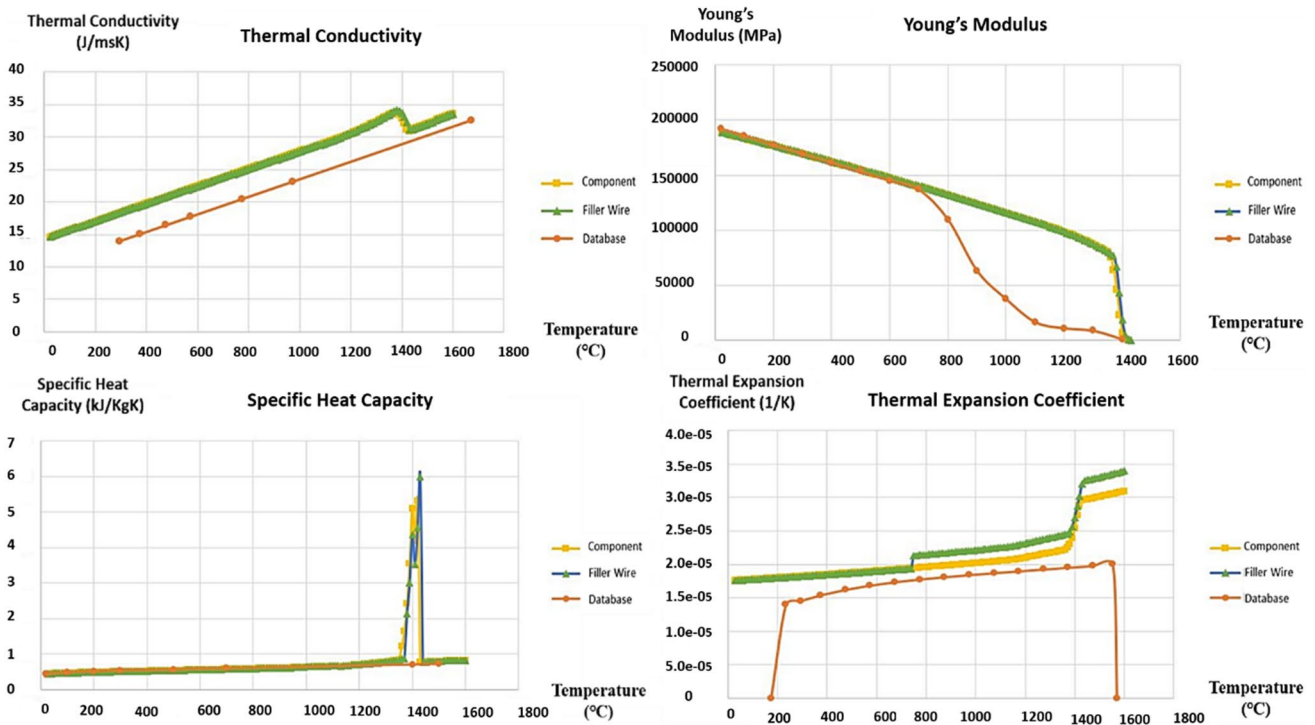
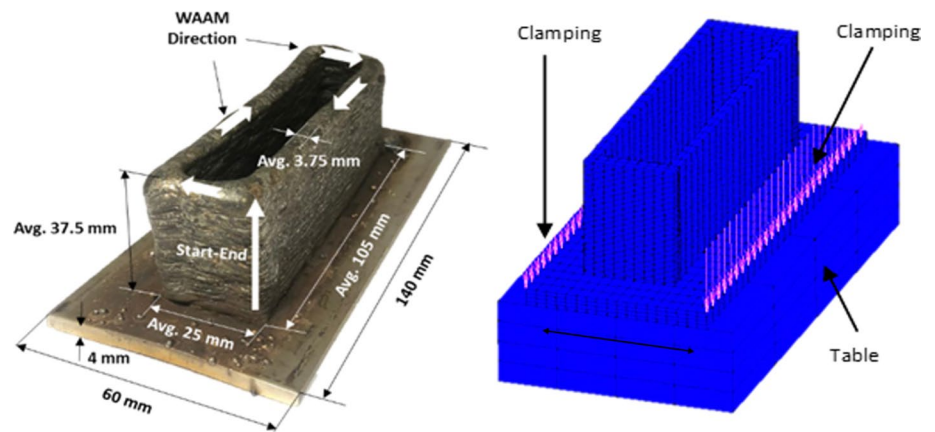


Fig. 5 Temperature-dependant material properties of SS316L

capacity. Apart from them, flow curves were modelled based on von Mises yield criteria created within strain rate from 0.001 to 1 s⁻¹. Figure 6 exhibits existing and generated flow curves at strain rate of 0.001 s⁻¹.

Apart from temperature-dependent material properties, flow curves were modelled based on von Mises yield criteria created within strain rate from 0.001 to 1 s⁻¹. Figure 6 exhibits existing and generated flow curves at strain rate of 0.001 s⁻¹.

Comparing the three flow curves, it is obvious by quick insight that there is non-significant difference between them. However, Fig. 7 details the slight difference at various

temperatures of 30 °C, 300 °C and 800 °C within the strain rate of 0.001/s. This small difference might lead to different result of distortion and residual stress.

3.2 Process parameter, heat source model and heat transfer coefficient

Process parameter model followed the actual parameters, while basic material properties such as latent heat, solidus and liquidus temperature are taken from material modelling software. Table 3 displays the WAAM process parameters and basic material property of SS316L.

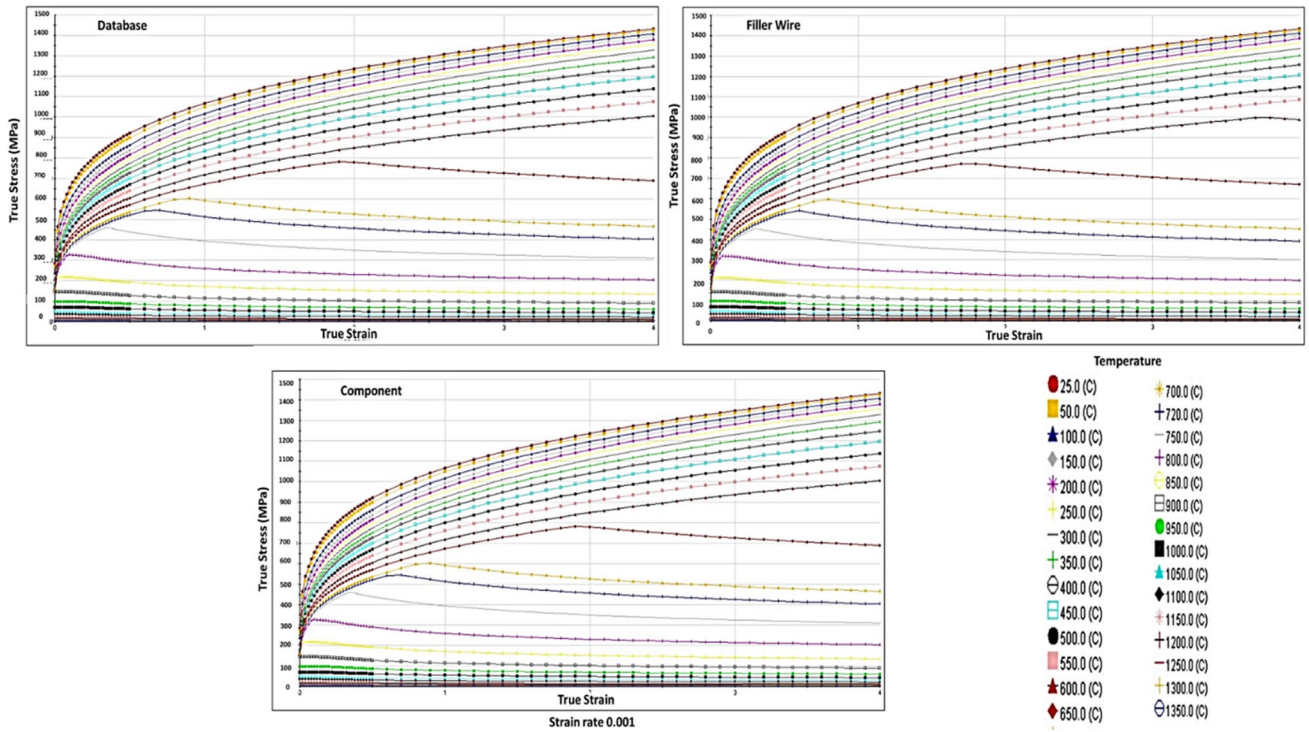


Fig. 6 Flow curve of evolved (upper left), original wire (upper right) and database material (below) at strain rate of 0.001 s⁻¹

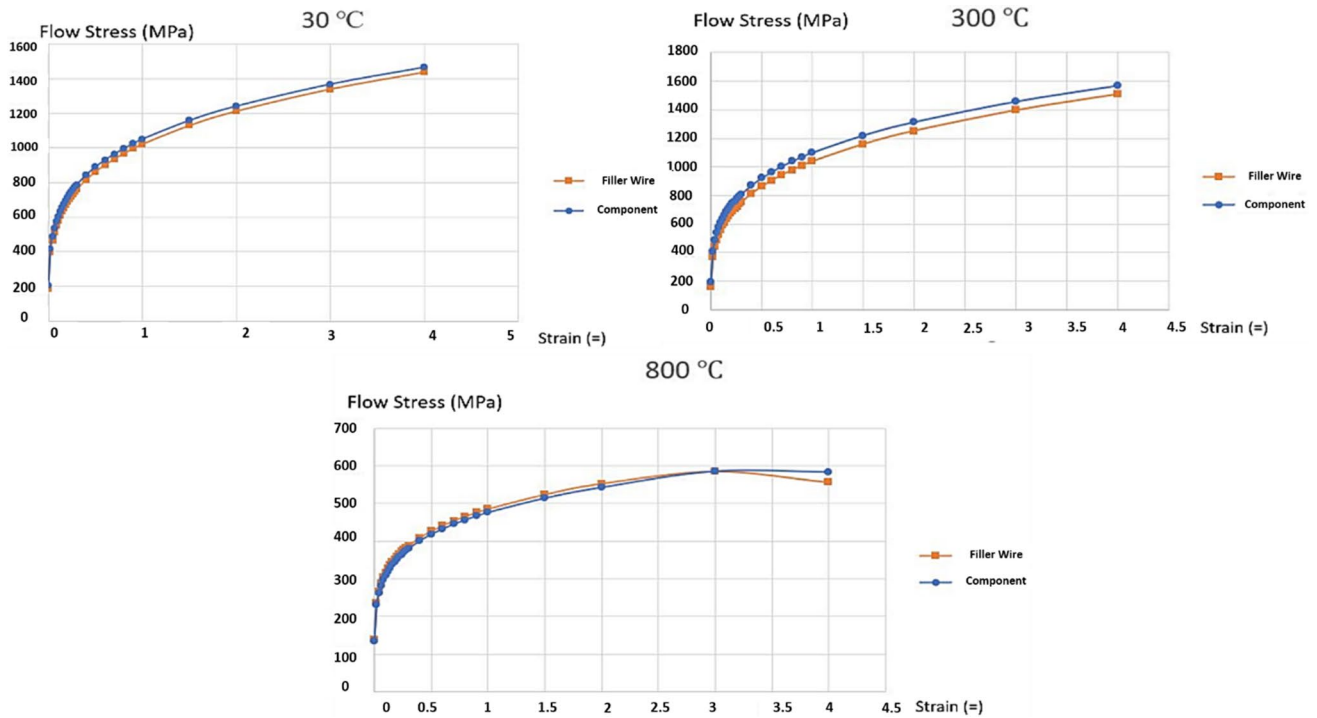


Fig. 7 Selected flow curve comparison of filler wire and component for 30, 300 and 800 degree at strain rate 0.001

Table 3 WAAM simulation parameters used in MSC Marc/Mentat

WAAM parameter	Value
Current, I (A)	88
Voltage, V (v)	21
Travel speed, v (mm/s)	7
Latent heat (J/kg)	256,400
Solidus temperature ($^{\circ}\text{C}$)	1279
Liquidus temperature ($^{\circ}\text{C}$)	1430

The crucial property of multi-layered welding simulation is the heat source modelling. In this WAAM simulation, Goldak's Double Ellipsoid model was selected as the moving heat source model which was very suitable for WAAM process sharing a similar concept with multi-layer GMAW simulation.

This heat source model is able to generate amount of heat during deposition of filler wire while controlling overall heat distributed in both substrate and weld bead of WAAM [26, 27]. This heat source model has also a function to generate the amount of heat while at the same time also enable itself to control the overall power poured into both substrate and weld beads.

In low penetration welding process such as GMAW, simulation with double-ellipsoidal heat source model can provide accurate result compared to experiments. The power density distribution of the moving heat source model is described in Eq. 1 and shown in Fig. 8, where a_f , a_r , b and c are the semi axis of the ellipsoid. The fractions of deposited head f_f and f_r represent the heat apportionments of the heat flux in the front and rear quadrants, provided that the condition $f_f + f_r = 2$ is fulfilled. The fractions can be assumed as $f_f = \frac{2a_f}{a_f + a_r}$ and $f_r = \frac{2a_r}{a_f + a_r}$ if volumetric heat source is considered [28]. The dimension of the heat source model assigned within WAAM simulation is exhibited in Table 4.

Table 4 Heat Source dimension in WAAM simulation

Heat source dimensions	Value
Width b (mm)	5
Depth c (mm)	5
Front length a_f (mm)	3
Rear length a_r (mm)	6

$$q_f(x, y, z) = \frac{6\sqrt{3}Qf_f}{a_f b c \pi \sqrt{\pi}} \exp\left(-\frac{3x^2}{a_f^2} - \frac{3y^2}{b^2} - \frac{3z^2}{c^2}\right) \quad (1)$$

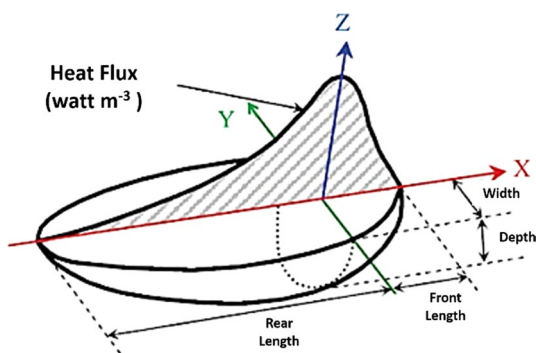
$$q_r(x, y, z) = \frac{6\sqrt{3}Qf_r}{a_r b c \pi \sqrt{\pi}} \exp\left(-\frac{3x^2}{a_r^2} - \frac{3y^2}{b^2} - \frac{3z^2}{c^2}\right)$$

To define suitable heat transfer coefficients, one of the methods was executed by calibrating the simulation-based result of temperature distribution to reflect the results from experiments. This kind of method was successfully implemented for WAAM simulation [30]. The adjustment was taken on similar positions as shown in Fig. 9 which also displays simulation results of the heated model of WAAM specimen using MSC Marc/Mentat based on three different material modelling methods. From the result of temperature distribution, it can be seen that each type of material data has different pattern of temperature distribution in term of peak temperature and the cooling pattern when the deposition reaches higher layers until the top. Using the material modelling of actual SS316L component and filler wire, the temperature distribution pattern has a closer peak and range compared to the experimental temperature distribution patterns, while simulation utilizing the database of SS316L has much lower peak temperature. Figure 10 exhibits the temperature distribution comparison graph of three different material models with experiments and the adjusted values of thermal transfer coefficients are shown in Table 5.

3.3 Mesh sensitivity analysis

Prior to the final implementation of the numerical computation, a mesh sensitivity analysis was carried out to ensure the best mesh size. Other important purpose of executing the mesh sensitivity analysis for this research is to find a trade-off between solution reliability and computational time. Mesh sensitivity study is a simple way to check potential singularity points in the mesh [31]. Many researches performing welding simulation incorporated mesh sensitivity analysis to define the optimized the element number which does not drastically alter the final result [32, 33].

In this research, the numerical simulation of WAAM process was only developed in two layers to simplify the mechanism of mesh sensitivity analysis and to reduce the overall

**Fig. 8** Goldak's double ellipsoidal heat source model [29]

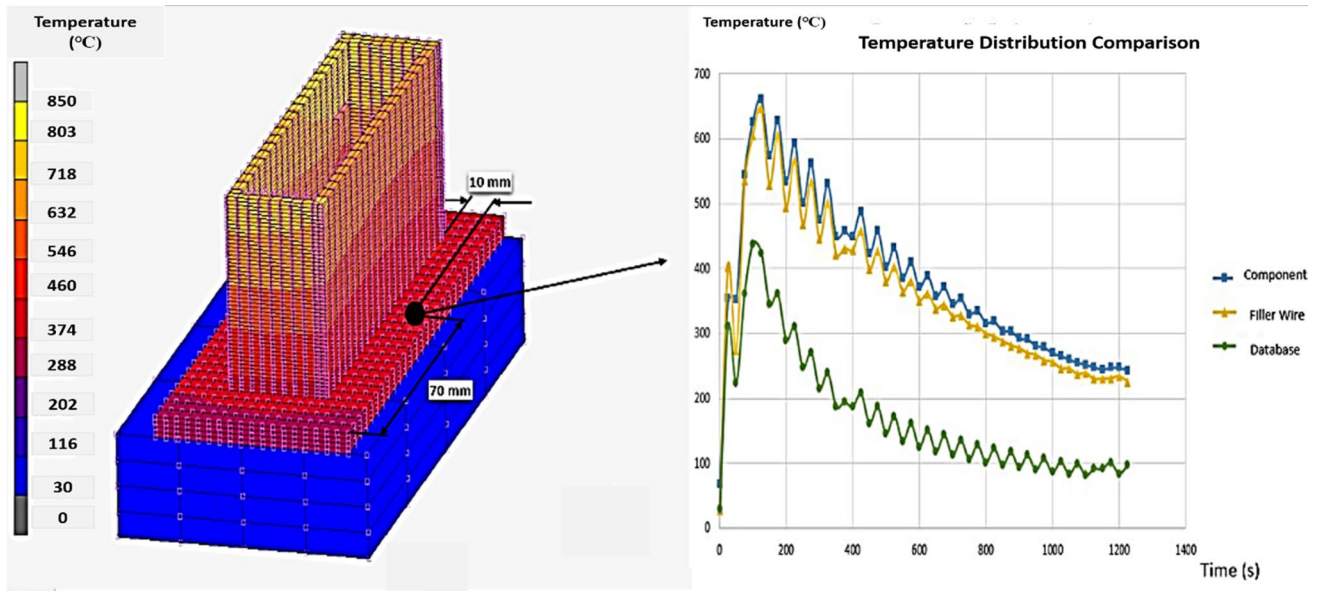


Fig. 9 Temperature distribution on substrate measured using numerical computation

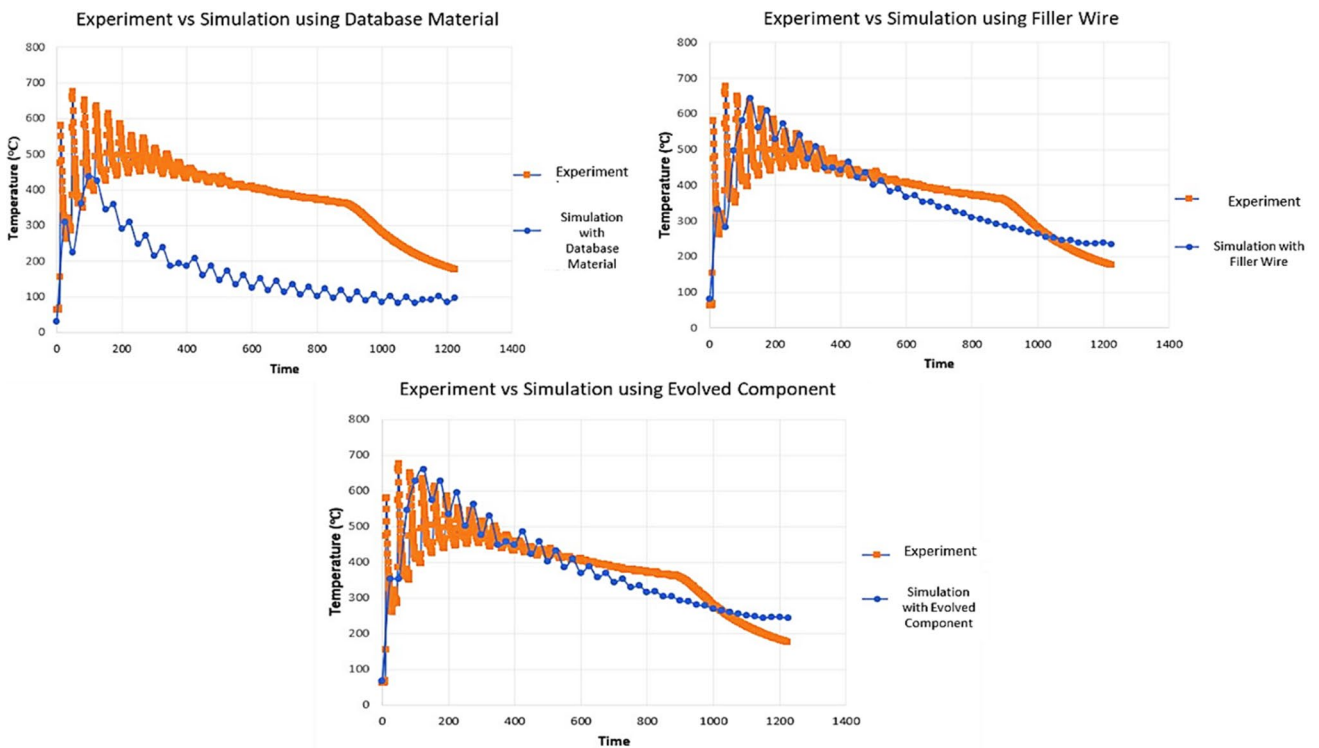


Fig. 10 Experimental and simulative temperature distribution based on various material models

computational time. The geometrical design of WAAM component which serves as the basis of sensitivity analysis is displayed in Fig. 11.

A comparison of different number of elements were conducted towards maximum temperature on similar node. The

method was to divide a finer mesh on each body consisting table, substrate and filler with the total number of elements from 1268 to 4888. The sensitivity analysis was executed by doing batch file methods in MSC Marc/Mentat by developing a user routine that enables to run multiple WAAM

Table 5 New adjusted thermal coefficients of WAAM product used in simulation

Numerical parameters	Value
Heat transfer coefficient, metal to metal (W/m ² K)	2500
Heat transfer coefficient, metal to environment (W/m ² K)	15
Emission coefficient	0.6

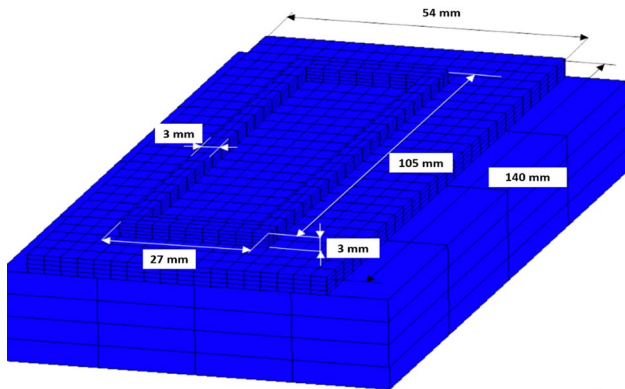


Fig. 11 Numerical WAAM model designed for mesh sensitivity analysis

Fig. 12 Mesh sensitivity graph for maximum temperature versus number of elements

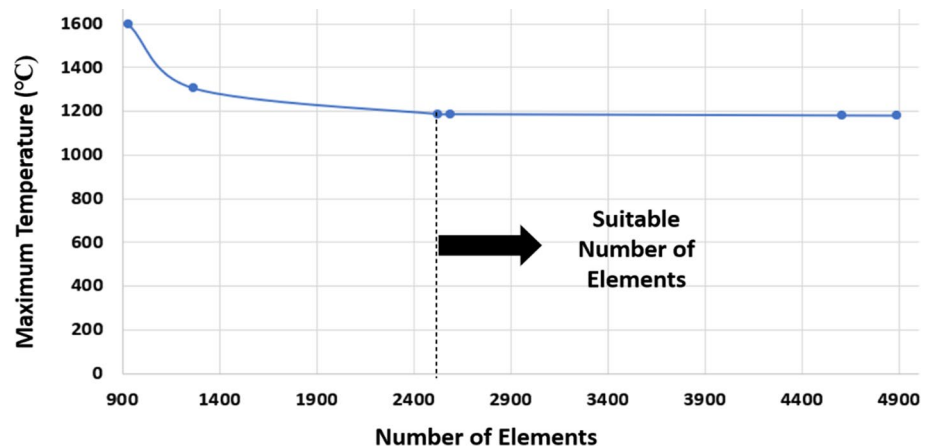


Table 6 Mesh sensitivity analysis numerical value for maximum temperature and computational time

Element set	Table	Substrate	Filler	Total number of elements	Wall time (s)	Convergence ration	Maximum temperature (°C)
Mesh set 1	8	800	122	930	135	0.0063	1598.3
Mesh set 2	32	1012	104	1268	140	0.0015	1304.5
Mesh set 3	64	2016	448	2528	144	0.0011	1186.9
Mesh set 4	128	2016	448	2592	145	0.00459	1186.9
Mesh set 5	128	4032	448	4608	597	0.01287	1181.1
Mesh Set 6	128	4032	728	4888	1436	0.0978	1180.4

simulation with different meshes at once. Figure 12 below exhibits the mesh sensitivity analysis graph between five different element sizes while Table 6 displays the numerical value of mesh sizes for each number of elements involved as well as computational time.

From the sensitivity analysis result displayed on both Fig. 12 and Table 6, it can be seen that the final result of temperature are influenced by the number of elements involved within the numerical FE analysis, but only after the number element of 2528, the maximum temperature value shows the similar range. The number of elements 2528 is the chosen mesh size since the number of elements after that just adds more computational time by 14% to 64% for each increasing element numbers.

4 Results of experiment and numerical computation

The accuracy of proposed model was to be analysed on the correlation of simulated and actual distortions. By utilizing CMM, the percentage of distortion on some measuring points were calculated. The distortion analysis is based on three different cases. The experimental result of WAAM can be seen in Fig. 10 stating the distortion based on five

points on substrate. The distortion patterns of three different simulations are displayed in Fig. 13.

Table 7 covers the overall comparison error percentage for all numerical models when it compared to the CMM result extracted by experimental WAAM process while the visualization of distortion result comparison is displayed by graphs within Fig. 15.

Based on the result displayed on Figs. 14, 15 and Table 7, it can be observed that the distortion occurred in numerical simulation using material database shows lower value compared to results which incorporate material model from filler wire and component. The numerical WAAM simulation based on scanned composition at evolved component indicates the lowest error percentage in term of distortion value compared to result from experiments. The difference of the distortion result might be also caused by the difference in preparation as well as experimental conditions that cannot be simulated by means of numerical computation. The final distortion results between experiment and numerical simulation in this research show lower error percentage on flow curve application on both evolved component ($\approx 11\%$) and filler wire ($\approx 16\%$) compared to software database ($\approx 22\%$).

Based on the current outcome of this research, it can be demonstrated that the results are relatively comparable to past investigation. A WAAM distortion analysis of Aluminium substrate was conducted leading to relative error margin of ca. 20% calculated using other commercial FEM software with a moving heat source model [34]. Another advanced research also performed an FE analysis to calculate distortion which also incorporated Goldak’s Double Ellipsoid heat source model. By taking the actual power distribution into account, the outcome showed an error percentage between 2 and 26% [35]. Equivalent research on residual distortion of commercial mild steel substrate showed a similar outcome pattern along the plates and relatively close value in comparison between numerical model with WAAM experiment [36].

5 Conclusion

The main objective of this research is to analyse the effect of various material property models on the simulation result and to suggest suitable one for future application. The simulation was carried out using nonlinear numerical

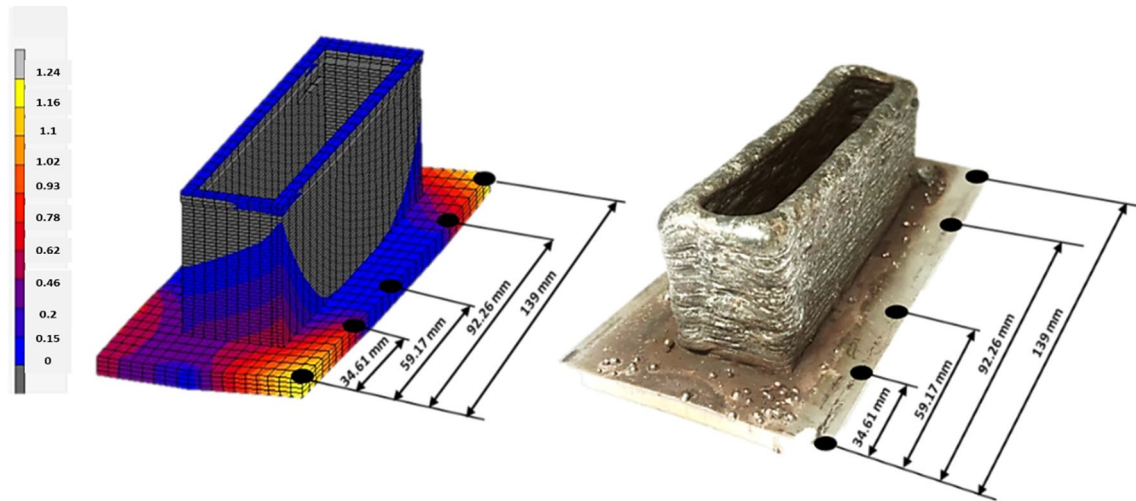


Fig. 13 Distortion measurement by substrate length displayed by experimental WAAM Simulation (left) and experimental WAAM (right)

Table 7 Distortion results of experiment and simulation of WAAM process

Approach	Location of measurement points (mm)					Average total distortion (mm)	Relative error percentage of total distortion (%)
	0	34.61	59.17	92.26	139		
Experiments (Std. Dev. $\sigma = 16\text{--}18 \mu\text{m}$)	1.37	0.95	0.59	0.23	0.69	0.76	–
Material model from software database	0.91	0.68	0.62	0.42	0.36	0.59	22.1
Material model from filler wire	0.99	0.99	0.59	0.25	0.39	0.64	15.9
Material model from component	1.14	0.86	0.41	0.20	0.78	0.68	11.1

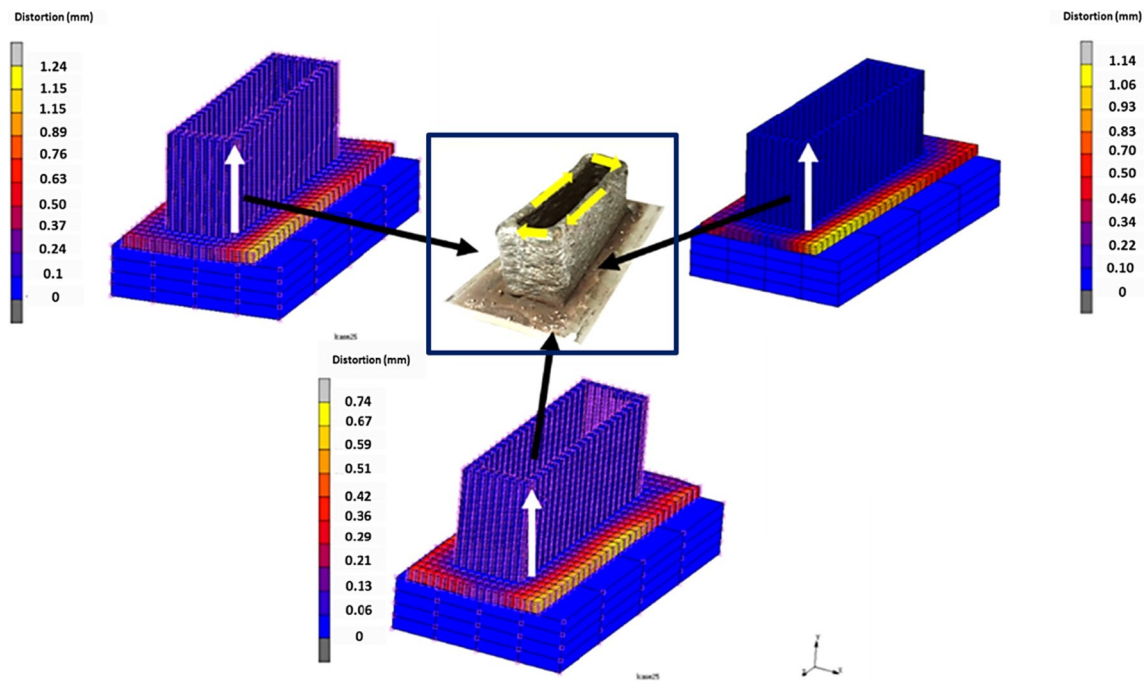
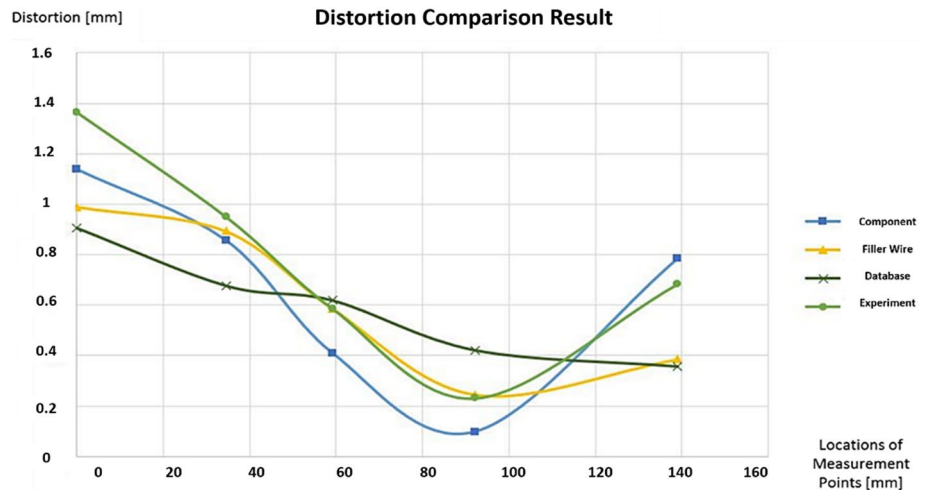


Fig. 14 Comparison of simulation result using material property model based on evolved component (upper left), filler wire (upper right) and software database (bottom) material

Fig. 15 Comparative distortion result between WAAM simulation and experiment



computation with plasticity model which covers wide range of temperature and strain rate. The study case for this investigation is hollow-shaped WAAM process which was modelled with simplified rectangular mesh geometry and simulated with most-popular Goldak’s double ellipsoid heat source model. The major heat transfer coefficients are adjusted based on actual experimental temperature distribution at similar point. Prior to final implementation of numerical simulation, a mesh sensitivity was to be analysed based on simplified geometrical model. Following contributions from this study can be summarized as follow:

- The numerical computation and experiment for twenty-five layers deposition of WAAM had been successfully executed as well as the experimental WAAM process leading to adjustment of heat transfer coefficient from metal to metal as well as from metal to air.
- Flow curves plays an significant role for predicting distortion and Gloldak’s double ellipsoid heat source model is suitable for simulating WAAM process.
- Rectangular bead geometry can save pre-processing step of simulation since the shape and mesh creation is not time consuming.

- A mesh sensitivity analysis is of important and should be conducted prior to final numerical simulation. It was decided to use numerical model with 2528 total number of elements with 1 mm mesh sizes due to constant maximum temperature value and ideal computational time.
- The high distortion is located closer to end-start position due to extensive heat.
- The substrate distortion analysed by numerical computation using evolved component and filler wire has a lower error percentage compared to experimental WAAM with 11.1% and 15.9% respectively, while the material property from software database has larger error percentage with 22.09%.
- Modelling software JMATPRO can produce suitable material property model for WAAM process.
- The error of simulation result can be caused by fluctuating parameters, shape inconsistency, material inhomogeneity etc.

As further recommendation, advanced research can be conducted using numerical computation verified with experiment on the assessment of plastic strain of substrate to predict the formability of base component.

Acknowledgements The authors would like to express their gratitude to staff member of Smart Manufacturing Research Institute (SMRI), Advanced Manufacturing Technology Excellence Centre (AMTEEx) and Research Interest Group: Advanced Manufacturing Technology (RIG:AMT) at Faculty of Mechanical Engineering, Universiti Teknologi MARA (UiTM) as well as Professorship of Virtual Production Engineering at Chemnitz University of Technology (CUT) in Germany. This research is supported by DAAD Germany with Project Code: 57525437 (Future Technology Additive Manufacturing), Geran Inisiatif Penyelidikan (GIP) from Phase 1/2019 with Project Code: 600-IRMI 5/3/GIP (073/2019) and Geran Konsortium Kecemerlangan Penyelidikan (Large Volume Additive Manufacturing/LVAM).

Compliance with ethical standards

Ethical statement We the undersigned declare that this manuscript is original, has not been published before and is not currently being considered for publication elsewhere.

We wish to confirm that there are no known conflicts of interest associated with this publication and there had been no significant financial support for this work that could have influenced its outcome.

We confirm that the manuscript had been read and approved by all named authors and that there are no other persons who satisfied the criteria for authorship but are not listed.

We further confirm that the order of authors listed in the manuscript had been approved by all of us.

We confirm that we have given due consideration to the protection of intellectual property associated with this work and that there are no impediments to publication, including the timing of publication, with respect to intellectual property. In so doing we confirm that we have followed the regulations of our institutions concerning intellectual property.

References

1. Erhunmwun ID, Ikponmwo UB. Review on finite element method. *J Appl Sci Environ Manag*. 2017;21(5):999. <https://doi.org/10.4314/jasem.v21i5.30>.
2. Sun Y, He M, Sun P. Numerical analysis of finite element method for a transient two-phase transport model of polymer electrolyte fuel cell. *Proc Comput Sci*. 2013;18:2167–76. <https://doi.org/10.1016/j.procs.2013.05.387>.
3. Gu J, et al. Deformation microstructures and strengthening mechanisms for the wire+arc additively manufactured Al-Mg4.5Mn alloy with inter-layer rolling. *Mater Sci Eng A*. 2018;712(January):292–301. <https://doi.org/10.1016/j.msea.2017.11.113>.
4. Rodrigues TA, Duarte V, Miranda RM, Santos TG, Oliveira JP. Current status and perspectives on wire and arc additive manufacturing (WAAM). *Materials*. 2019;12:7. <https://doi.org/10.3390/ma12071121>.
5. Li JZ, Alkahari MR, Rosli NAB, Hasan R, Sudin MN, Ramli FR. Review of wire arc additive manufacturing for 3D Metal Printing. *Int J Autom Technol*. 2019;13(3):346–53. <https://doi.org/10.1016/j.jmapro.2018.08.001>.
6. Mehnen J, Ding J, Lockett H, Kazanas P. Design study for wire and arc additive manufacture. *Int J Prod Dev*. 2014;19(1–3):2–20. <https://doi.org/10.1007/s00170-019-03959>.
7. Ding J, Colegrove P, Mehnen J, Williams S, Wang F, Almeida PS. A computationally efficient finite element model of wire and arc additive manufacture. *Int J Adv Manuf Technol*. 2014;70(1–4):227–36. <https://doi.org/10.1504/IJPD.2014.060028>.
8. Denlinger ER, Michaleris P. Effect of stress relaxation on distortion in additive manufacturing process modeling. *Addit Manuf*. 2016;12:51–9. <https://doi.org/10.1016/j.addma.2016.06.011>.
9. Panda B, Shankwar K, Garg A, Savalani M. Evaluation of genetic programming-based models for simulating bead dimensions in wire and arc additive manufacturing. *J Intell Manuf*. 2016;30:809–20. <https://doi.org/10.1007/s10845-016-1282-2>.
10. Hu Z, Qin X, Li Y, Yuan J, Wu Q. Multi-bead overlapping model with varying cross-section profile for robotic GMAW-based additive manufacturing. *J Intell Manuf*. 2019;40:1–15. <https://doi.org/10.1007/s10845-019-01501-z>.
11. Roman J, Colegrove P, Williams S. Analytical model for distortion prediction in wire + arc additive manufacturing. *Residual Stress*. 2018;6:277–82. <https://doi.org/10.21741/9781945291890-44>.
12. Graf M, Hälsig A, et al. Thermo-mechanical modelling of wire-arc additive manufacturing (WAAM) of semi-finished products. *Metals Open Access Metallurgy J*. 2018;8:12. <https://doi.org/10.3390/met8121009>.
13. Adebayo A, Stephen JT. Effect of distortion on wire and arc additive manufacturing straight walls. *J Build Construct Plann Mater*. 2017;2(1):1–7. <https://doi.org/10.18488/journal.84.2017.21.1.7>.
14. Hui H, Ninshu M, et al. Towards arge-scale simulation of residual stress and distortion in wire and arc additive manufacturing. *Addit Manuf*. 2020;34:5. <https://doi.org/10.1016/j.addma.2020.101248>.
15. Montevocchi F, et al. Finite element mesh coarsening for effective distortion prediction in wire arc additive manufacturing. *Addit Manuf*. 2017;18:24–33. <https://doi.org/10.1016/j.addma.2017.10.010>.
16. Park SC, Banf HS, Seong WJ. Effect of material properties on angular distortion in wire arc additive manufacturing: experimental and computational analysis. *Materials*. 2020;13:6. <https://doi.org/10.3390/ma13061399>.
17. Turner R, Schroeder F, Ward RM, Brooks JW. The importance of materials data and modelling parameters in an FE simulation of linear friction welding. *Adv Mater Sci Eng*. 2014;2014:1–9. <https://doi.org/10.1155/2014/521937>.

18. Lindgren L-E. Finite element modeling and simulation of welding: improved material. *J Therm Stress*. 2001;24(3):195–231. <https://doi.org/10.1080/014957301300006380>.
19. Pryl D, Cervenka J. Material properties investigation using numerical weld investigation. *AIP Proc Confer*. 2015;3(1):102–8. <https://doi.org/10.1016/j.proeng.2015.06.0365>.
20. Yehorov Y, Da Silva LJ, Scottu A. Exploring the use of switch-back for mitigating homoepitaxial unidirectional grain growth and porosity in WAAM of aluminium alloys. *Int J Adv Manuf Technol*. 2019;104(1–4):1581–92. <https://doi.org/10.1007/s00170-019-03959>.
21. He T, Yu S, Shi Y, Dai Y. High-accuracy and high-performance WAAM propeller manufacture by cylindrical surface slicing method. *Int J Adv Manuf Technol*. 2019;105:203–12. <https://doi.org/10.1007/s00170-019-04558>.
22. Wang L, Wei H, Xue JX, Debroy T. Special features of double pulsed gas metal arc welding. *J Mater Process Technol*. 2017;251:369–75. <https://doi.org/10.1016/j.jmatprotec.2017.08.039>.
23. Banshi PA, Rajeev K. Challenges in application of pulse current gas metal arc welding process for preparation of weld joint with superior quality. *Int J Eng Res Technol*. 2016;5:1. <https://doi.org/10.17577/IJERTV5IS010350>.
24. Guo J, Xu X, Jepson MAE, Thomson RC. Influence of weld thermal cycle and post weld heat treatment on the microstructure of MarBN steel. *Int J Press Vessels Pip*. 2019;174:13–24. <https://doi.org/10.1016/j.ijpvp.2019.05.010>.
25. Rankumar KD, Gokul Kumar K. Characterization of metallurgical and mechanical properties on the multi-pass welding of Inconel 625 and AISI 316L. *J Mech Sci Technol*. 2014;29(3):1039–47. <https://doi.org/10.1007/s12206-014-1112-4>.
26. Hamahmy M, Deiab I. Review and analysis of heat source models for additive manufacturing. *Int J Adv Manuf Technol*. 2019;104:1–16. <https://doi.org/10.1007/s00170-019-04371-0>.
27. Bae DH, Kim CH, Cho SY, Hong J, Tsai CL. Numerical analysis of welding residual stress using heat source models for the multi-pass weldment. *KSME Int J*. 2002;16(9):1054–64. <https://doi.org/10.1007/BF02984424>.
28. Lundback A. Finite element modelling and simulation of welding of aerospace components [Master Thesis]. Sweden: Lulea University of Technology; 2003.
29. Abid M, Qarni MJ. 3D thermal finite element analysis of single pass girth welded low carbon steel pipe-flange joints. *Turk J Eng Environ Sci*. 2009;33:281–93. <https://doi.org/10.3906/muh-0912-6>.
30. Graf M, et al. Numerical simulation of metallic wire arc additive manufacturing (WAAM). *AIP Conf Proc*. 2018;1960:1. <https://doi.org/10.1063/1.5035002>.
31. D V, Durairaj R, . 3D finite element simulation of temperature distribution, residual stress and distortion on 304 stainless steel plates using GTA welding. *J Mech Sci Technol*. 2016;30:67–76. <https://doi.org/10.1007/s12206-015-1208-5>.
32. Kumar TS, Atikukke N, Kannan R. Thermal cycling effects on the creep-fatigue interaction in type 316LN austenitic stainless steel weld joint. *Int J Press Vessels Pip*. 2019;178:1040. <https://doi.org/10.1016/j.ijpvp.2019.104009>.
33. Hu Z, Qin X, Shao T. Welding thermal simulation and metallurgical characteristics analysis in WAAM for 5crnimo hot forging die remanufacturing. *Proc Eng*. 2017;207:2203–8. <https://doi.org/10.1016/j.proeng.2017.10.98>.
34. Jinlong J, Yue Z, Mingye D, Aiping W, Quan L. Numerical simulation on residual stress and deformation for WAAM parts of alluminium alloy based on temperature function method. *China Welding*. 2020;29(2):1–8. <https://doi.org/10.12073/j.cw.20191101002>.
35. Montevocchi F, Scippa A, Campatelli G. Finite element modelling of Wire-arc-additive-manufacturing process. *Proc CIRP*. 2016. <https://doi.org/10.1016/j.procir.2016.08.024>.
36. Hui H, Jian C, et al (2018) Stress and distortion simulation of additive manufacturing process by high performance computing. In: *Proceeding of the ASME 2018 Pressure Vessels and Piping Conference (PVP 2018)*. <https://doi.org/10.1115/PVP2018-85045>

Publisher's Note Springer Nature remains neutral with regard to jurisdictional claims in published maps and institutional affiliations.